

Further contributions on the two-dimensional flow in a sudden expansion

By N. ALLEBORN¹, K. NANDAKUMAR²,
H. RASZILLIER¹ AND F. DURST¹

¹Lehrstuhl für Strömungsmechanik, Cauerstr. 4, 91058 Erlangen, Germany

²Department of Chemical Engineering, University of Alberta, Edmonton, Alberta, Canada, T6G 2G6

(Received 18 December 1995 and in revised form 19 July 1996)

Two-dimensional laminar flow of an incompressible viscous fluid through a channel with a sudden expansion is investigated. A continuation method is applied to study the bifurcation structure of the discretized governing equations. The stability of the different solution branches is determined by an Arnoldi-based iterative method for calculating the most unstable eigenmodes of the linearized equations for the perturbation quantities. The bifurcation picture is extended by computing additional solution branches and bifurcation points. The behaviour of the critical eigenvalues in the neighbourhood of these bifurcation points is studied. Limiting cases for the geometrical and flow parameters are considered and numerical results are compared with analytical solutions for these cases.

1. Introduction

Two-dimensional, laminar flow of an incompressible, Newtonian fluid in a symmetric, sudden expansion has been the subject of several previous investigations. Experimental results have been reported by Cherdron, Durst & Whitelaw (1978), Durst, Pereira & Tropea (1993) and Fearn, Mullin & Cliffe (1990) for expansion ratios D between the outlet and inlet heights of 2:1 and 3:1. At sufficiently low Reynolds numbers Re the experiments report a steady, symmetric flow with two recirculation zones of equal size in the corners of the expansion. The length of these recirculation zones increases with increasing Reynolds number.

Even in the creeping flow limit, there must be recirculation zones, called Moffatt vortices, at the corners. These have been largely ignored in previous studies on sudden expansion. Using high-resolution numerical schemes (i.e. successive grid refinement) Collins & Dennis (1976) have tracked these weak viscous eddies in curved, triangular ducts. They are of minor consequence in determining the nonlinear structure of the solutions, but an important indicator of the numerical accuracy as the size and strength of these vortices are very small and they do not reveal themselves readily in numerical calculations. We compare our numerical solutions with the analytical results of Moffatt (1964) to serve as validation of our choice of the number of grid points and the grid distribution.

For higher Reynolds numbers, the experiments reveal the symmetric flow yielding gradually to a pair of stable, asymmetric flows, which retain the two-dimensional, stationary character. The two recirculation zones in these flows achieve different

lengths. The values of the Reynolds number for the onset of asymmetric flows, reported by experiment, scatter over a wide range: for example Cherdron *et al.* (1978) report the transition to occur at $Re = 185$ based on the maximum inlet velocity and the corresponding inlet channel height for an expansion ratio of 2 : 1, while Durst *et al.* (1993) report the critical value to be around $Re = 125$ for the same expansion ratio, when Re is based on the maximum inlet velocity and the inlet height. For $Re > 600$ the flow eventually becomes transient and quantitative experimental data on the frequency *vs.* Re is available in both Cherdron *et al.* (1978) and Fearn *et al.* (1990) on such transient flows.

In a definitive study, Fearn *et al.* (1990) show, using both numerical and experimental tools, that at a certain critical Reynolds number (which depends on the expansion ratio) the unique, symmetric solution bifurcates supercritically at a pitchfork point; the symmetric solution loses stability at this singular point and a pair of stable, asymmetric solutions emerge. Since the symmetry-breaking point is structurally unstable, the presence of even a slight degree of asymmetry in the experiments or the numerical model makes the transition between the symmetric and non-symmetric solution appear as a smooth one, with the second non-symmetric solution being disconnected from the primary branch. The pitchfork unfolds into a limit point which is very sensitive to such slight imperfections in experiments or computations. Their study reaffirms the other, earlier observations concerning transition between the symmetric and non-symmetric flows and it clarifies the reason for the sensitive nature of the singular point in both experiments and computations.

Shapira, Degani & Weihs (1990) consider a *gradual* expansion with a *constant* slope of angle α in the expansion zone. They discuss stability issues, but make no attempt to determine the structure of the many stationary solutions beyond the first bifurcation point. Instead they rely on direct simulation (or integration) of the linearized, transient, two-dimensional equations to determine the stability of two-dimensional base flows. The novel feature in their work is the manner in which the stability of the least-stable mode is determined, using an energy-based method. In their work there is no evidence of multiplicity of stable, non-symmetric solutions, nor of any further limit points on the non-symmetric branches.

In yet another seminal work, Sobey & Drazin (1986) explore the connection between the bifurcation structure of Jeffery–Hamel flows (JH flow: the two-dimensional flow of given rate Q and Reynolds number $Re = Q/\nu$ in a wedge of angle 2α from a source or sink in its edge) and the flows in a *periodic*, plane channel with a *smooth* expansion and contraction. Results from the bifurcation theory are rigorously applied to the JH flows and their stability is determined from a model problem derived from the JH flows, instead of solving the complete eigenvalue problem. For the channel flows, a direct, time-dependent numerical simulation was used which permits access to all stable solution branches as well as any time-periodic solutions, but cannot reveal the solution structure of any unstable solutions. The bifurcation diagram for the channel flow is more complicated than in other studies. The essential findings in their work are: (a) while in the channel flow the first bifurcation point, with Re as bifurcation parameter, is *supercritical*, in the JH flow (at a fixed α) it is *subcritical*; (b) additional limit points on the asymmetric solution branches of the channel flow are uncovered and bracketed by extensive numerical simulations. The relevance of the work of Sobey & Drazin (1986) in the present context arises from the fact that the JH flows can be looked upon as limit configurations of sudden or gradual expansion flows (expansion ratio $D \rightarrow \infty$).

In the present paper we explore the bifurcation structure of the steady solution

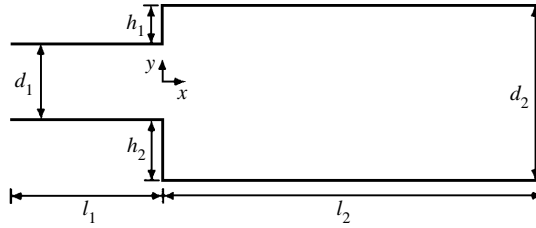


FIGURE 1. Two-dimensional duct with a sudden expansion.

manifold of two-dimensional sudden expansion flow in detail by numerical methods. Finite difference approximations of the equations of motion in the stream function–vorticity form are constructed. A suitable stretching transformation is used to cluster the grid points near the walls and corners. The sensitivity of the solution to different types of approximations for the vorticity boundary conditions on the wall and corner points, as well as at the outlet, is examined. The Newton method provides access to the Jacobian and hence makes possible the computation of eigenvalues to determine the linear stability; a continuation method with branch switching (Allgower & Georg 1990) allows us to compute both stable and unstable branches. Arnoldi-based iterative methods are used to track the variation of the eigenvalues of the least-stable modes with respect to Reynolds number. Yet another motivation was a recent numerical study (Teschauer 1994) using a commercial code FIDAP, where evidence of a second pair of non-symmetric solution branches was found, suggesting the presence of a second bifurcation point on the unstable, symmetric solution branch for an expansion ratio of 1 : 2. This and other bifurcation points have the same location to within 2 ~ 4%. Although the bifurcation structure of the stationary solutions has some similarity with that found in the Taylor–Couette flow (Pfister *et al.* 1987) for a short annulus, the stability picture is quite different.

The variation of the solution manifold with the expansion ratio D is tracked, with an attempt to extrapolate to $D \rightarrow \infty$ by a computation for $D = 1000$ and by comparisons with the submerged jet and the JH flow. Whereas the classical Bickley jet turns out to be an unsuitable limit for the present problem, the numerical solution for $D = 1000$ (and $Re = 1$) shows good agreement with the JH flow for $\alpha = \pi/2$.

2. Problem formulation

Figure 1 shows the geometry of the channel being considered. It is characterized by the expansion ratio

$$D = \frac{d_2}{d_1} \quad (2.1)$$

and the expansion asymmetry

$$a = \frac{h_1 - h_2}{d_1}, \quad (2.2)$$

which can be used to model slight asymmetries occurring in an experimental arrangement. The lengths of the entrance and outflow regions, $L_1 = l_1/d_1$ and $L_2 = l_2/d_1$ respectively, have to be chosen sufficiently long so that the flow profiles far away upstream and downstream can be regarded as fully developed. Using d_1 as the length scale, there are four dimensionless geometrical parameters (D, a, L_1, L_2). While D and

a have profound influence on the flow and bifurcation structure, L_1 and L_2 have much less influence as long as they are sufficiently large.

The spatial variables x and y are normalized by d_1 and the velocity vector $\mathbf{u} = (u, v)$ is scaled with the maximum velocity u_0 at the inlet. The steady flow of an incompressible viscous fluid is governed by the continuity equation

$$\nabla \cdot \mathbf{u} = 0 \quad (2.3)$$

and the Navier–Stokes equation

$$(\mathbf{u} \cdot \nabla) \mathbf{u} = -\nabla p + \frac{1}{Re} \nabla^2 \mathbf{u} \quad (2.4)$$

where p is the non-dimensional pressure. The Reynolds number is defined by

$$Re = \frac{u_0 d_1}{\nu} \quad (2.5)$$

where u_0 is the maximum velocity at the inlet and ν is the kinematic viscosity. The condition $\mathbf{u} = \mathbf{0}$ is imposed at solid walls and a fully developed one-dimensional Poiseuille flow

$$\mathbf{u}(y) = ((1 - 4y^2/d_1^2), 0)^T \quad (2.6)$$

is assumed on the inlet. The Reynolds number is given as

$$Re = \frac{3Q}{2\nu}, \quad (2.7)$$

in terms of the flow rate $Q = \frac{2}{3}u_0 d_1$ per unit channel width. The outflow boundary conditions will be discussed later.

In the special case $h_1 = h_2$, i.e. $a = 0$, the duct possesses a reflection symmetry about the centreline $y = 0$. Equations (2.3) and (2.4) and the boundary conditions are invariant under the transformation

$$\begin{aligned} y &\rightarrow -y \\ v &\rightarrow -v \end{aligned} \quad (2.8)$$

with the other quantities left unchanged. Hence, if $(u(x, y), v(x, y))$ represents a solution of (2.3)–(2.4), then the mirror image $(u(x, -y), -v(x, -y))$ is a solution of the governing equations as well. In particular symmetric solutions are characterized by

$$\begin{pmatrix} u(x, y) \\ v(x, y) \end{pmatrix} = \begin{pmatrix} u(x, -y) \\ -v(x, -y) \end{pmatrix}. \quad (2.9)$$

As a consequence of this symmetry, only symmetric solutions may appear alone, whereas asymmetric solutions have to appear in pairs.

3. Numerical solution

For a two-dimensional problem a velocity field

$$\mathbf{u} = \frac{\partial \psi}{\partial y}, \quad v = -\frac{\partial \psi}{\partial x}, \quad (3.1)$$

induced by a streamfunction ψ , satisfies the continuity equation (2.3). Eliminating the pressure terms in the Navier–Stokes equations results in the vorticity equation

$$\frac{\partial \psi}{\partial y} \frac{\partial \omega}{\partial x} - \frac{\partial \psi}{\partial x} \frac{\partial \omega}{\partial y} = \frac{1}{Re} \nabla^2 \omega \quad (3.2)$$

where

$$\omega = \frac{\partial u}{\partial y} - \frac{\partial v}{\partial x}. \quad (3.3)$$

The streamfunction and vorticity are related by

$$\omega = \nabla^2 \psi. \quad (3.4)$$

The boundary conditions for the streamfunction are

$$\psi = \pm \frac{1}{3} \quad (3.5)$$

on the solid upper and lower walls respectively and

$$\psi(y) = y - \frac{4}{3}y^3 \quad (3.6)$$

at the inlet. Roache (1972) proposes different outflow boundary conditions such as

$$\frac{\partial \psi}{\partial x} = 0 \quad (3.7)$$

or

$$\frac{\partial^2 \psi}{\partial x^2} = 0. \quad (3.8)$$

For the vorticity ω , boundary conditions on a solid wall do not exist. But since the no-slip condition also yields the normal derivative of the streamfunction $\partial \psi / \partial n = 0$, this can be used to derive approximate boundary conditions for ω . Various first- and second-order-accurate finite difference approximations for the vorticity at a solid surface are given by Roache (1972), using the values of ψ and ω at one or two interior points ($w + 1$ and $w + 2$ respectively) close to a wall point w . A Taylor expansion of ψ on the solid wall together with the no-slip condition for the velocity gives

$$\omega_w = \frac{2(\psi_{w+1} - \psi_w)}{\Delta n^2} + O(\Delta n) \quad (3.9)$$

up to first-order terms in Δn denoting the normal distance of point $w + 1$ from w . Extending this expansion to higher-order terms, the following second-order-accurate equation can be obtained:

$$\omega_w = \frac{3(\psi_{w+1} - \psi_w)}{\Delta n^2} - \frac{1}{2}\omega_{w+1} + O(\Delta n^2). \quad (3.10)$$

Another approach is to use a third-order polynomial interpolation of the streamfunction near the wall, yielding

$$\omega_w = \frac{-7\psi_w + 8\psi_{w+1} - \psi_{w+2}}{2\Delta n^2} + O(\Delta n^2), \quad (3.11)$$

for the vorticity, which also has a second-order truncation error. At the sharp convex corner of the sudden expansion at $x = 0$ a unique boundary value for the vorticity does not exist. Roache (1972) recommends using multiple values as well as using a unique value obtained by interpolation. The condition

$$\frac{\partial \omega}{\partial x} = 0 \quad (3.12)$$

for the vorticity is imposed on the outflow boundary. Calculations using different approximations for boundary and outflow conditions have been carried out in order to make sure that the choice of these conditions does not influence the solution structure significantly.

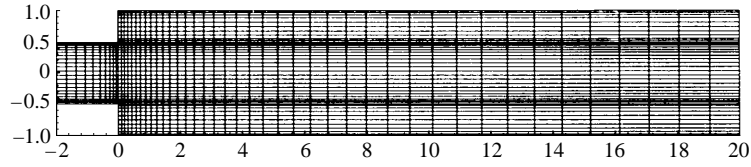


FIGURE 2. Mesh for the sudden expansion flow.

The equations of motion (3.2) and (3.4) are discretized using a five-point finite differencing scheme. Stretching transformations are used to generate a cluster of grid points in regions of flow where sharp changes in the flow field are expected (see figure 2). Discretizing the equations for the change gives the nonlinear algebraic system

$$H(\psi_i, \omega_i, Re, D, a, L_1, L_2) = 0, \quad i = 1.., N, \quad (3.13)$$

with unknowns (ψ_i, ω_i) in the N grid points. The system additionally depends on several parameters, such as Re or a . In order to study the structural changes in the solution manifold with the variation of these parameters, a continuation method is applied which exploits the smooth dependence of the solutions on them.

In the present work the arclength predictor–corrector method described by Allgower & Georg (1990) is used. The sparse linear system of equations arising from the Newton–Raphson iteration in the corrector step is solved by LU decomposition using the package SPARSPAK (Chu *et al.* 1984). The advantage of a direct solver lies in the fact that the determinant of the Jacobian of (3.13) which changes sign at turning and simple bifurcation points can be conveniently obtained as a byproduct of the factorization and used as an indicator for these points.

4. Linear stability

In order that a flow described by the governing equations is observed in nature or experiment it has to be stable under small perturbations. To investigate the stability of the various configurations for the channel flow obtained by solution of the equations (3.2), (3.4) or (3.13), a linear stability analysis is carried out. The configuration of the steady basic flow (Ψ, Ω) is perturbed by small time-dependent quantities:

$$\left. \begin{aligned} \tilde{\psi}(x, y, t) &= \Psi(x, y) + \psi(x, y, t), \\ \tilde{\omega}(x, y, t) &= \Omega(x, y) + \omega(x, y, t). \end{aligned} \right\} \quad (4.1)$$

For an infinitesimally small perturbation, the equations of motion can be linearized:

$$\left. \begin{aligned} \Psi_x \frac{\partial \omega}{\partial y} + \Omega_y \frac{\partial \psi}{\partial x} - \Psi_y \frac{\partial \omega}{\partial x} - \Omega_x \frac{\partial \psi}{\partial y} + \frac{1}{Re} \nabla^2 \omega &= \frac{\partial \omega}{\partial t}, \\ \omega - \nabla^2 \psi &= 0. \end{aligned} \right\} \quad (4.2)$$

The linearized problem is now solved for $\psi(x, y, t)$ and $\omega(x, y, t)$ using a normal mode decomposition:

$$\left. \begin{aligned} \psi(x, y, t) &= \hat{\psi}(x, y) e^{\sigma t}, \\ \omega(x, y, t) &= \hat{\omega}(x, y) e^{\sigma t}. \end{aligned} \right\} \quad (4.3)$$

with a complex eigenvalue σ and eigenvectors $\hat{\psi}(x, y)$ and $\hat{\omega}(x, y)$. Substituting ansatz (4.3) into (4.2) and discretizing leads to the generalized algebraic eigenvalue problem

$$\mathbf{J}(\Psi, \Omega) \mathbf{y} = \sigma \mathbf{M} \mathbf{y}. \quad (4.4)$$

The matrix \mathbf{J} represents the Jacobian matrix of (3.13) evaluated for the basic flow and \mathbf{M} is a singular diagonal matrix arising from the right-hand side of (4.2).

The basic flow (Ψ, Ω) is infinitesimally stable if $\text{Re}\{\sigma\} < 0$ holds for all eigenvalues σ of (4.4), i.e. if all perturbations in (4.1) will decay with time. If there is at least one eigenvalue with $\text{Re}\{\sigma\} > 0$, the corresponding eigenmode (4.3) will grow as $t \rightarrow \infty$ and the basic flow is unstable. In the context of a bifurcation analysis the dependence of σ on a parameter like Re is of interest.

Some conclusions on the stability of a flow configuration can already be drawn from a sign change of $\det\{\mathbf{J}\}$, mentioned in §3, without explicitly looking at the spectrum of (4.4). At a turning point or a simple bifurcation point the principle of exchange of stability applies for a stable flow (Keller 1987): a real eigenvalue of equation (4.4) passes through $\sigma = 0$ from $\sigma < 0$ (stable flow) to $\sigma > 0$ (unstable flow), thereby a change of sign in $\det\{\mathbf{J}\}$ occurs.

However, if the solution is already unstable or if a pair of conjugate-complex eigenvalues crosses the imaginary axis (Hopf bifurcation), the sign change of $\det\mathbf{J}$ alone does not give sufficient information about an exchange of stability. For these cases it is necessary to calculate at least the rightmost part of the spectrum of (4.4). An effective algorithm for this purpose is a shift-and-invert method combined with the Arnoldi algorithm for calculating parts of the spectrum (Natarajan & Acrivos 1993; Saad 1992). The generalized eigenvalue problem (4.4) is transformed into a standard eigenvalue problem

$$(\mathbf{J} - \tau\mathbf{M})^{-1}\mathbf{M}\mathbf{y} = \hat{\sigma}\mathbf{y} \quad (4.5)$$

with a complex shift parameter τ . The eigenvalues $\hat{\sigma}$ are related to those of (4.4) by

$$\hat{\sigma} = \frac{1}{\sigma - \tau}. \quad (4.6)$$

This standard problem is then solved by a restarted, iterative Arnoldi method which essentially is a sophisticated extension of the power iteration method and allows a number of eigenvalues $\hat{\sigma}$ of largest magnitude to be calculated (Saad 1992). By transformation (4.6) these are the eigenvalues σ of equation (4.4) closest to the shift τ .

The explicit calculation of the inverse matrix $(\mathbf{J} - \tau\mathbf{M})^{-1}$ in the matrix vector products $\mathbf{z} = (\mathbf{J} - \tau\mathbf{M})^{-1}\mathbf{M}\mathbf{x}$ which are repeatedly required by the Arnoldi method for a given \mathbf{x} can be avoided by using the LU-decomposition of $(\mathbf{J} - \tau\mathbf{M})$ and solving

$$(\mathbf{J} - \tau\mathbf{M})\mathbf{z} = \mathbf{M}\mathbf{x} \quad (4.7)$$

for \mathbf{z} . This requires only the matrix-vector product $\mathbf{M}\mathbf{x}$ and one forward and backward substitution in the factorized system. For a real shift τ this can be done efficiently by SPARSPAK. A useful implementation of the Arnoldi-method is provided by the package ARPACK (Lehoucq, Sorensen & Vu n.d.) which was used in the present work.

5. Moffatt eddies

Before proceeding to a detailed study of the flow patterns over a wide range of Reynolds numbers, the limiting case $Re = 0$ will be considered. In this case recirculation zones of finite size are known to remain in the corners of the expansion (see figure 3). The analytical work of Moffatt (1964) shows that an infinite sequence of closed eddies of decreasing strength exists near a sharp corner with an angle

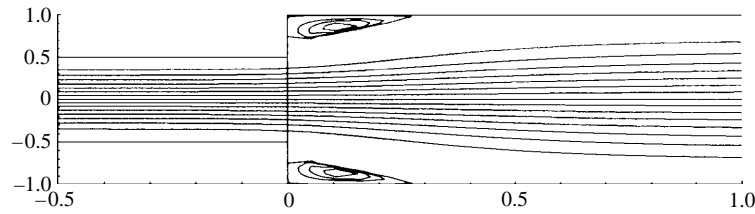


FIGURE 3. Moffatt eddies in the corners of the sudden expansion ($Re = 0, D = 2, a = 0, L_1 = 2, L_2 = 40$).

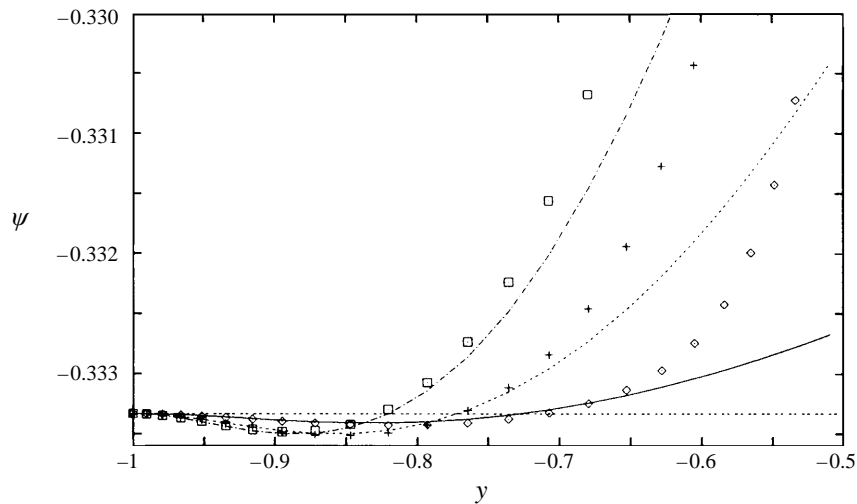


FIGURE 4. Streamfunction near the corner for an expansion ratio $D = 2$. —/ \diamond : analytical/numerical solution at $x = 0.05$, - - -/+ at $x = 0.10$, $\cdots\cdots$ / \square at $x = 0.15$, dashed horizontal line: $\psi = 1/3$.

$2\alpha < 146^\circ$. These have come to be known as Moffatt eddies, and they represent a solution of (3.2) and (3.4) for $Re = 0$. Moffatt (1964) derives an expression in polar coordinates with origin in the corner for the lowest-order term of the complex streamfunction:

$$\psi_c(r, \vartheta) \approx K r^\lambda (\cos((\lambda - 2)\alpha) \cos(\lambda\vartheta) - \cos(\lambda\alpha) \cos((\lambda - 2)\vartheta)) \quad (5.1)$$

which obeys

$$\psi_c(r, \pm\alpha) = 0, \quad \frac{\partial \psi_c}{\partial \vartheta}(r, \pm\alpha) = 0, \quad (5.2)$$

since the complex value of λ is fixed by

$$\lambda \tan \lambda\alpha = (\lambda - 2) \tan(\lambda - 2)\alpha. \quad (5.3)$$

In the case of a sudden expansion $2\alpha = \pi/2$ holds. The complex coefficient K has to be determined by matching the real part of (5.1) with the flow far away from the corner. In the present paper this has been done by using one value of the numerically obtained streamfunction both above and below the separation streamline.

In figure 4 the appropriately normalized asymptotic approximation of the flow in the lower corner is compared with the numerical solution for the expansion ratio $D = 2$ at different locations x . The numerical results agree well with the analytical

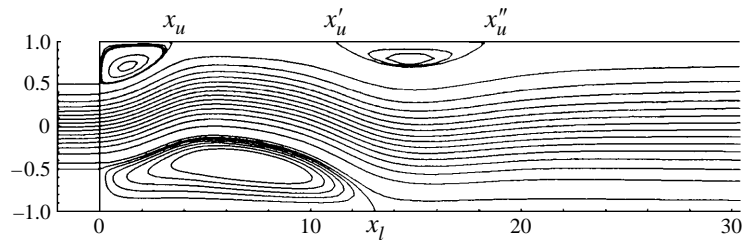


FIGURE 5. Asymmetric solution for $Re = 550$. x_u is the position of the reattachment point on the upper wall and x_l on the lower wall ($D = 2, a = 0, L_1 = 2, L_2 = 40$).

solution (5.1) for the corner eddies. With the grid size used in this work only the first corner eddy could be resolved numerically for $Re = 0$. Moffatt (1964) demonstrated that even for finite Reynolds numbers the flow in a sufficiently small neighbourhood of the corner can still be described by the creeping flow approximation. As the Reynolds number increases the size of the corner eddies also increases, the first and biggest one representing the main recirculation zone. For higher Reynolds numbers, this first recirculation zone induces a cascade of smaller Moffatt eddies of which two could be resolved numerically in the present work.

6. Bifurcation analysis

In this section the application of the above-mentioned numerical algorithms to study the flow in a plane channel with a sudden expansion will be described. Calculations were carried out first for a fixed expansion ratio $D = 2$ and the influence of the parameters of the numerical model such as mesh size or boundary conditions was studied. The dependence of the solutions on the expansion ratio D were then investigated and finally the limit case $D \rightarrow \infty$ has been considered.

6.1. Flow at expansion ratio $D = 2$

In order to have a quantitative measure for the characterization of a flow configuration, particularly of its asymmetry, and to illustrate the many flow configurations in a convenient way graphically, an appropriate functional has to be chosen. The x -coordinates of the reattachment points of the corner recirculation zones on the upper and lower walls are convenient choices for such a functional, since they can be determined quite easily (figure 5) and their difference $\Delta x = x_u - x_l$ clearly is an indicator of asymmetry in the flow.

The results of the numerical calculations for $D = 2$ on a 200×100 mesh are shown in figure 6. In the range $0 < Re < 800$ two symmetry-breaking pitchfork bifurcations were detected at $Re_{c1} = 218$ and $Re_{c2} = 542$. For $Re < Re_{c1}$ there is a unique, symmetric and stable flow configuration (with $\Delta x = 0$). This configuration loses stability at $Re_{c1} = 218$. The critical Reynolds number found for this first bifurcation point agrees well with the experimental and numerical results by Shapira *et al.* (1990) and Teschauer (1994).

Continuing the unstable symmetric solution to higher Reynolds numbers, a second bifurcation point was found at Re_{c2} which has not been reported before. At this bifurcation point the sign change of $\det\{\mathbf{J}\}$ alone is not sufficient to indicate whether the symmetric solution regains stability by crossing it, i.e. the positive eigenvalue crosses the origin back into the left complex half-plane again, as e.g. observed in

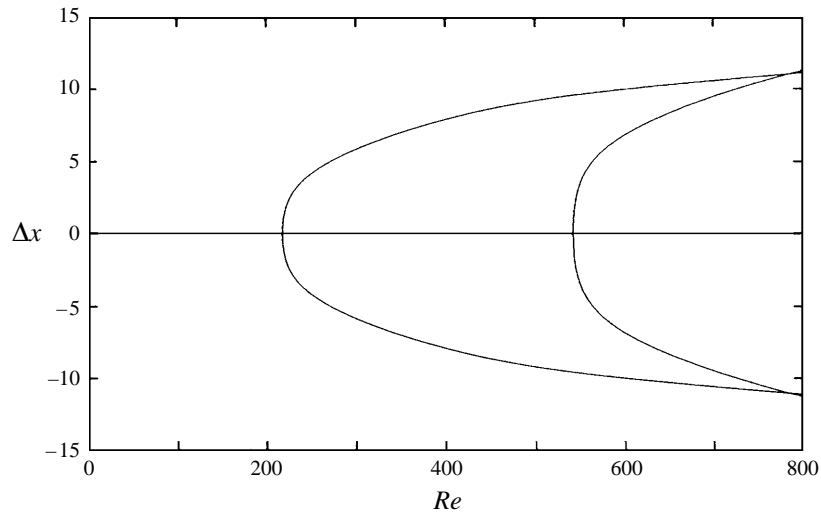


FIGURE 6. Bifurcation diagram for the sudden expansion flow. Expansion ratio $D = 2$, $a = 0$, $L_1 = 2$, $L_2 = 40$, and 200×100 grid points.

Taylor–Couette flow (Pfister *et al.* 1987), or whether it remains unstable, i.e. a second eigenmode becomes unstable.

A more detailed stability picture of the various symmetric and asymmetric branches of figure 6 is obtained by calculating a set of least-stable modes corresponding to the rightmost eigenvalues of the spectrum of equation (4.4). Figure 7(*a, b*) shows the transition to instability due to bifurcation for the symmetric solution. For $Re = 210 < Re_{c1}$ all eigenvalues are in the left half-plane and the solution is stable. With increase of the Reynolds number the rightmost eigenvalue moves to the right and crosses the origin of the complex plane at Re_{c1} . For $Re > Re_{c1}$ this eigenvalue is positive, i.e. the mode associated with this eigenvalue grows in time.

On increasing the Reynolds number further, a second eigenvalue of the symmetric solution moves to the right and crosses the origin at $Re_{c2} = 542$, leading to a second unstable mode. In figure 7(*c, d*) the relevant parts of the spectrum of the symmetric solution are shown for $Re = 540 < Re_{c2}$ and $Re = 560 > Re_{c2}$. The results indicate that the symmetric solutions remain unstable beyond the second bifurcation point. Also the asymmetric solutions of the second bifurcation point are unstable (figure 7*e*), so that from this point no physically observable two-dimensional flows originate.

The asymmetric solutions arising from the first bifurcation point are stable. In the experiments these solutions become unstable and time periodic at higher Reynolds numbers ($Re \approx 625$, Durst *et al.* 1993) and the existence of a Hopf bifurcation on the asymmetric branch was postulated. The behaviour of the rightmost eigenvalue was traced up to $Re = 800$ (figure 7*f*) and the asymmetric solutions were found to be stable to the two-dimensional perturbations applied, in agreement with the numerical results for two-dimensional flow of Fearn *et al.* (1990). In their work a transition to time-periodic flow via three-dimensional effects was observed experimentally. Streamline plots of the solution on the symmetric branch and upper part of the asymmetric branch of the first and second bifurcation are shown in figure 8 at $Re = 768$.

A few remarks on the influence of the numerical model on the previous results are in order. For studying the flow in a range of Reynolds numbers the lengths of the inlet and outlet segments of the channel have to be chosen sufficiently long to

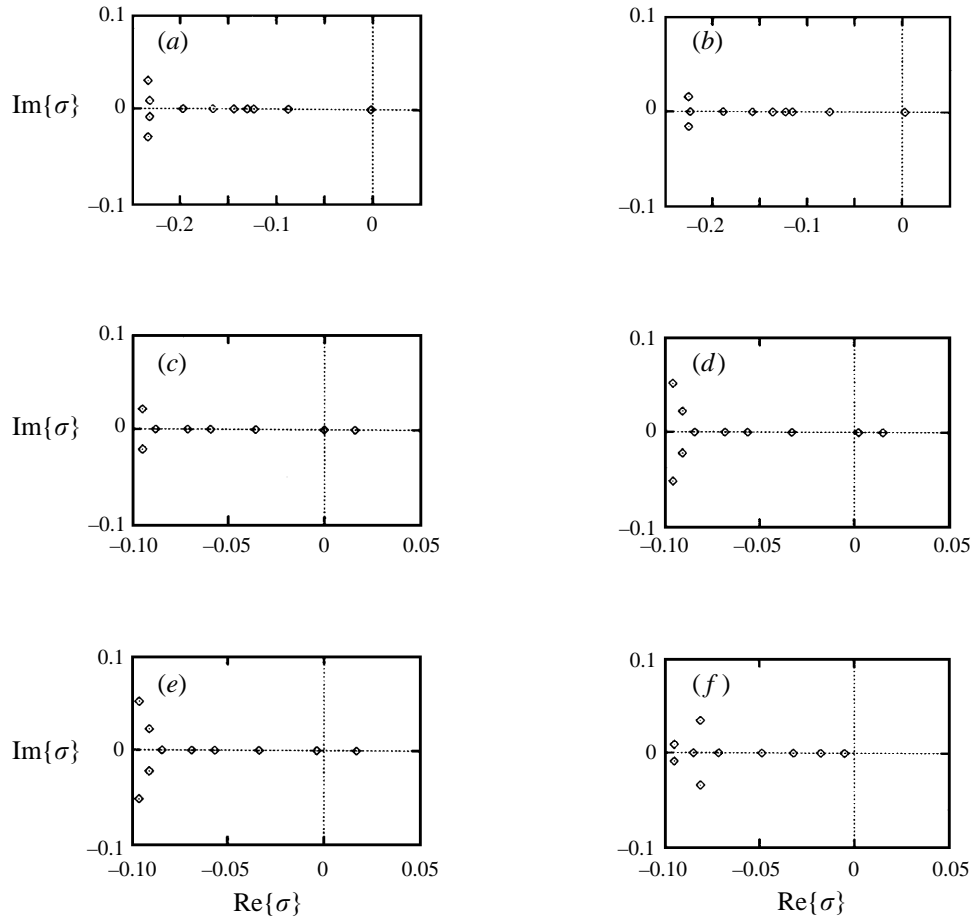


FIGURE 7. Eigenvalues in the complex plane. Symmetric solutions: (a) $Re = 210$, (b) $Re = 230$, (c) $Re = 540$, (d) $Re = 560$. Asymmetric solutions: (e) $Re = 560$ (2nd bifurcation), (f) $Re = 800$ (1st bifurcation). Shift $\lambda = 0$.

allow a fully developed flow at the outlet boundary and to avoid an influence of the expansion region. A first estimation of the length of the outflow region is taken from Schlichting (1968). The entrance length for a channel with uniform velocity distribution is $L_e \approx 0.035DRe$, giving $L_e \approx 56$ for $Re \leq 800$ and $D = 2$. Repeated calculations at $Re = 800$ with different lengths of the outflow L_2 showed that this length could be reduced to $L_2 = 40$ without affecting the location of bifurcation points and separation lengths significantly, keeping the relative error of those values less than 0.2% on a given mesh.

The global influence of the mesh size on the state functions is shown in figure 9. The influence of the mesh size is maximal in a neighbourhood of a singular point and, generally, increases with increasing Reynolds number.

The calculations were repeated on a refined mesh until the relative error of the separation length and of the bifurcation points between two meshes was less than 1% in the range of Reynolds numbers considered. On the finest (200×100) mesh different approaches for the approximation of ω on solid walls (3.9)–(3.11) and on the convex corners of the expansion (multivalued *vs.* interpolation) were investigated as well as different outflow boundary conditions (3.7)–(3.8). The relative error between

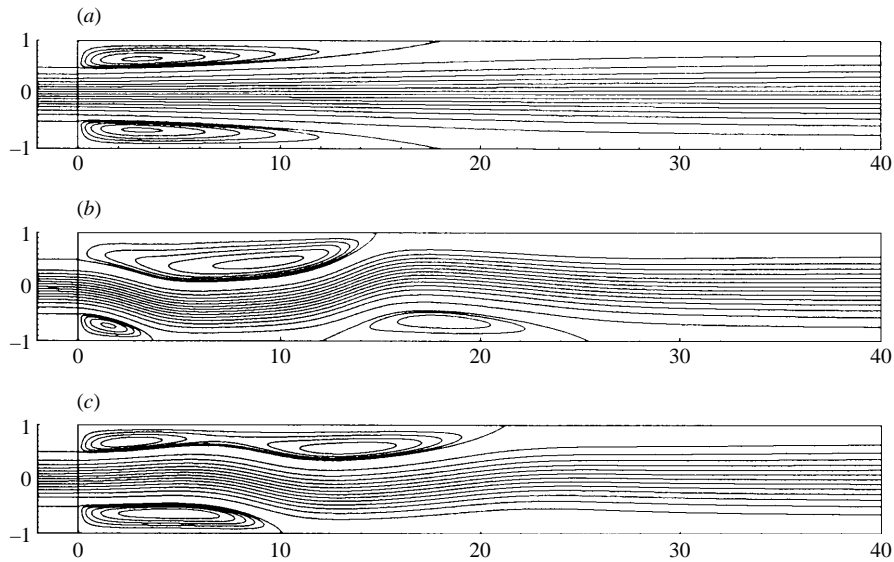


FIGURE 8. Streamline plots for $Re = 786$: (a) symmetric solution (unstable), (b) asymmetric solution (stable branch arising from 1st bifurcation), (c) asymmetric solution (unstable branch arising from 2nd bifurcation).

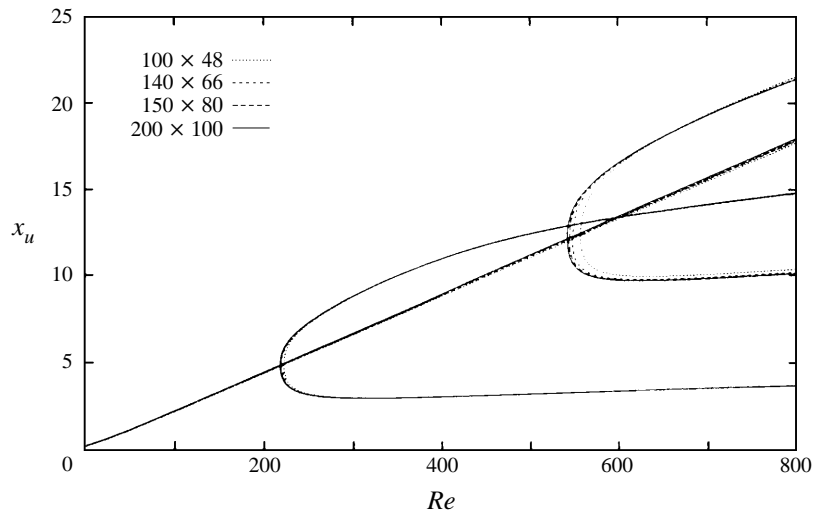


FIGURE 9. Bifurcation diagram for the sudden expansion flow. x_u vs. Re for different mesh sizes.

different numerical boundary conditions was found to be less than 0.2%. Although the influence of the mesh size and numerical boundary conditions on the bifurcation diagram (i.e. the state function in its dependence on Re), is quite small, the impact of grid refinement on the spectrum of the stability problem is dramatic, as expected. Figure 10 shows for the spectrum of symmetric solutions at $Re = 560$ that the three most unstable eigenvalues are sufficiently accurate on different grids, so that there is no significant change in the stability picture. The influence of the numerical boundary conditions on the relevant part of the spectrum is rather small and can be neglected. The inner part of the spectrum, however, is much more sensitive to the mesh size and is shifted as the grid is refined. A stronger grid dependence of the inner

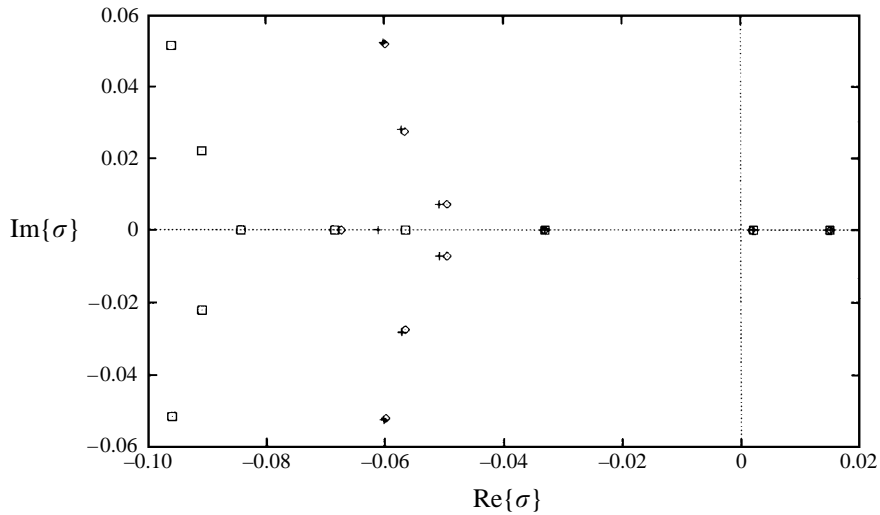


FIGURE 10. Influence of grid size and boundary conditions on the rightmost part of the spectrum. Symmetric solution, $Re = 560$. \diamond , 12300 points, 2nd-order vorticity boundary condition +; 12300 points, 1st-order vorticity boundary condition; \square , 21500 points, 2nd-order vorticity boundary condition.

part of the spectrum is mathematically expected from the increase of the degrees of freedom implied by grid refinement. The fact that it appears relatively close to the eigenvalue responsible for stability in this problem compared to other problems, see e.g. Natarajan & Acrivos (1993), could be attributed here possibly to the steep gradients of the vorticity near the convex corners. The vorticity changes significantly in these regions when more grid points are concentrated there, even though the solution is sufficiently accurate in all other parts of the channel. The singularity of the vorticity at the convex corner implies significant changes in the Jacobian matrix \mathbf{J} in (4.4), eventually accounting for this grid dependence of the spectrum.

When an arbitrary, small geometric asymmetry of the flow domain (expansion asymmetry $a \neq 0$) is introduced, the bifurcation picture changes qualitatively, as depicted in figures 11(a) and 11(b) for the functionals x_u and x_l . The bifurcation points unfold through the symmetry breaking, i.e. the branches intersecting at a bifurcation point become disconnected. The situation is sometimes referred to as an imperfect bifurcation. When the Reynolds number is gradually increased from small values, the asymmetry Δx of the flow increases smoothly, but with larger gradients in a neighbourhood of the critical Reynolds number Re_c for symmetric (perfect) geometry. The sign of the asymmetry parameter a prescribes whether it is the recirculation zone on the upper wall that grows while the lower one shrinks or vice versa.

The symmetry-breaking bifurcation point unfolds to a simple turning point on the disconnected lower branch in figure 11(a) (upper branch in 11b accordingly) with the lower part of this branch being stable, corresponding to the lower asymmetric branch of the symmetric geometry. The upper part emerging from the turning point is unstable due to the principle of exchange of stability. The asymmetry influences the second bifurcation at $Re_{c2} = 542$ in a similar way as the first one. In an experiment small geometric imperfections always cause a bifurcation diagram similar to figure 11 and disconnected stable branches can only be reached e.g. by starting the flow impulsively at the appropriate Reynolds number or by temporarily introducing artificial perturbations (Fearn *et al.* 1990). With increasing asymmetry the turning

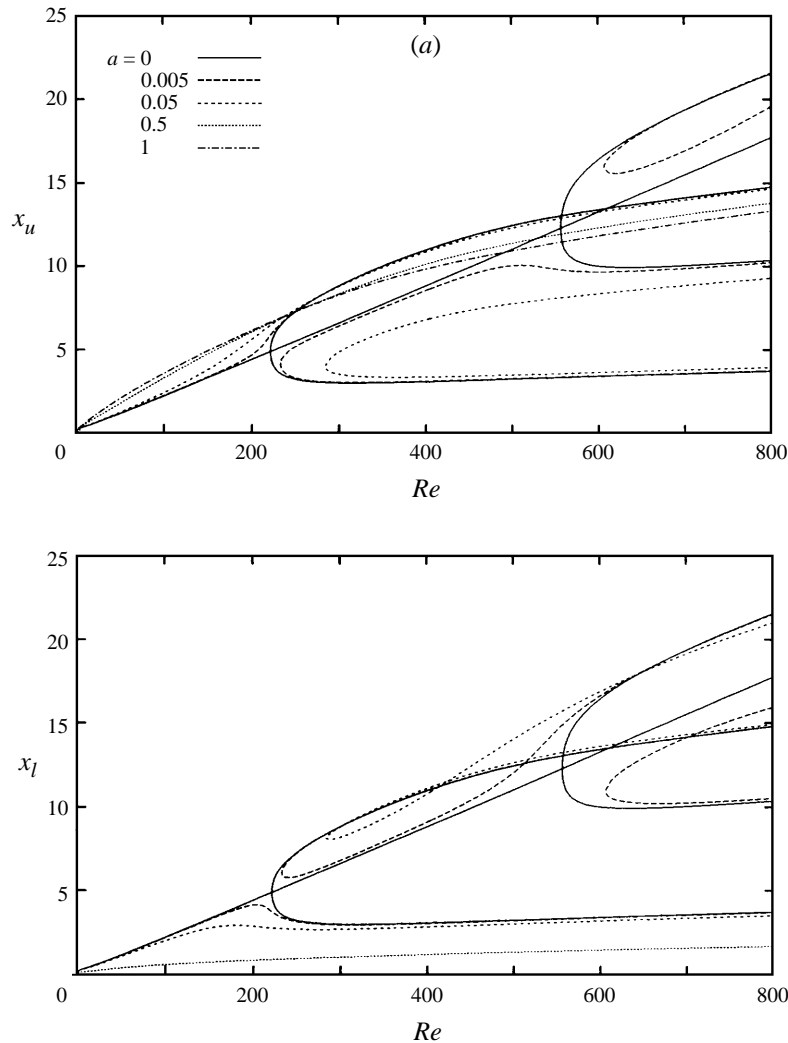


FIGURE 11. Dependency of the location x_u (a) and x_l (b) of the reattachment points on the upper and lower wall respectively on Re for different expansion asymmetries a (location of x_l and x_u according to figure 5).

points of the disconnected branches move towards higher Reynolds numbers and the branch $x_u(Re)$ in figure 11 asymptotically reaches the case of a backward-facing step ($a = 1$) with an expansion ratio 1 : 2 between inflow and outflow channel height, while $x_l(Re) = 0$ in this case.

Similar results to those in figure 11 could be obtained by introducing various kinds of asymmetries into the algorithm such as e.g. an asymmetric distribution of grid points. Inherent asymmetries of this kind in the numerical scheme account for the imperfect bifurcations found by Durst *et al.* (1993) and Sobey & Drazin (1986).

6.2. Influence of the expansion ratio D

For increasing expansion ratio the symmetry-breaking bifurcation occurs at lower Reynolds numbers. Figure 12 shows for ratios $D = 2, 3$ and 5 that the asymmetry of the solutions, measured by Δx , grows more rapidly at higher D and the curvature of

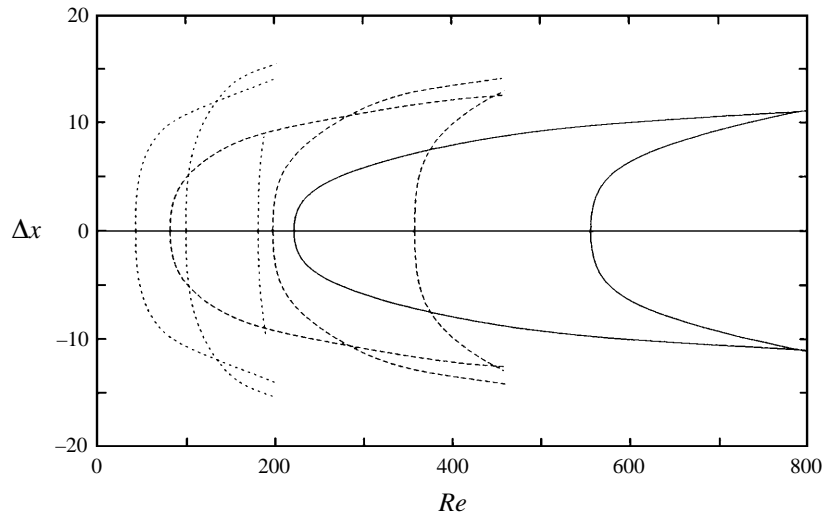


FIGURE 12. Dependence of the bifurcation diagram on the expansion ratio:
 $D = 2$ (—), $D = 3$ (---), $D = 5$ (⋯⋯⋯).

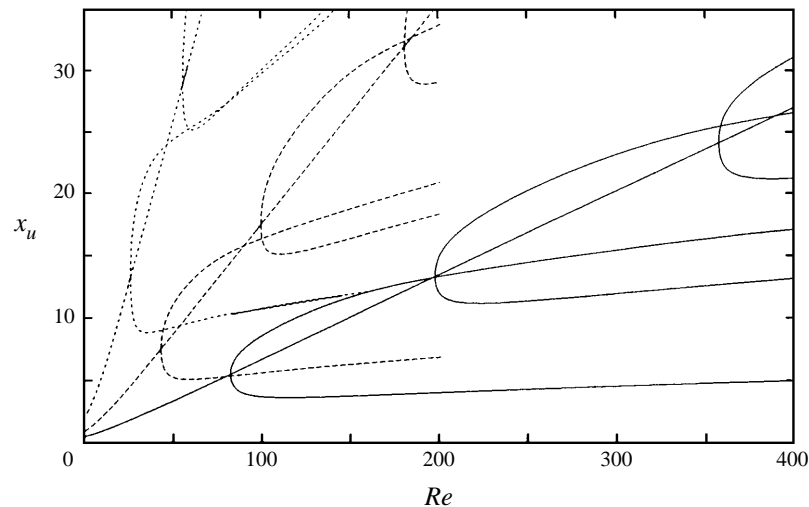


FIGURE 13. Dependence of the separation length x_u on the expansion ratio:
 $D = 3$ (—), $D = 5$ (---), $D = 10$ (⋯⋯⋯).

the asymmetric branches flattens near the bifurcation point. The distance between the first and second bifurcation points decreases. Additional bifurcation points connecting unstable branches have been found and the results suggest an infinite sequence of such points for $Re \rightarrow \infty$. The calculations however were confined to a range of Reynolds numbers containing the first two points because in experiments the flow becomes three-dimensional and transient for higher Re (Durst *et al.* 1993; Fearn *et al.* 1990). Not only does the asymmetry Δx of the solution grow more rapidly with increasing D but also the separation lengths x_u and x_l (figure 13). The Moffatt eddies, giving finite separation lengths for $Re = 0$ increasing with D in figure 13, have already been discussed in §5.

Figure 14 summarizes the dependence of the critical Reynolds numbers Re_{c1} and

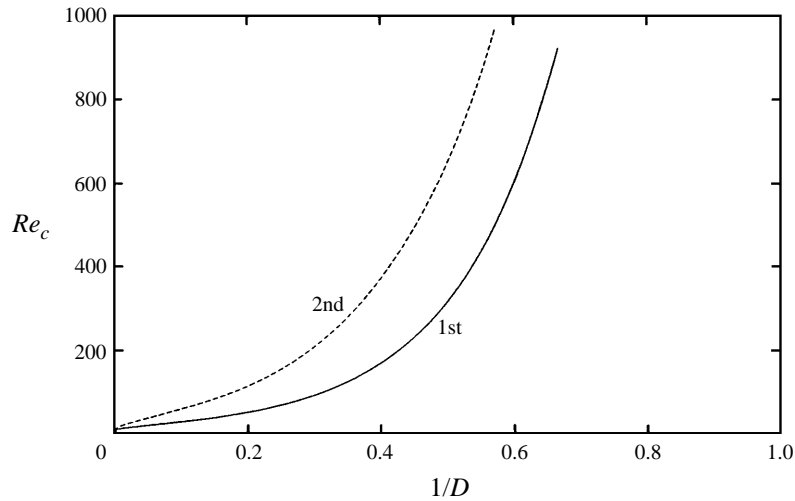


FIGURE 14. Reynolds number of the 1st (—) and 2nd (- - -) bifurcation points *vs.* reciprocal expansion ratio $1/D$.

Re_{c2} on the expansion ratio D . For $D \rightarrow 1$ the Reynolds numbers of both bifurcation points move rapidly towards high Reynolds numbers. In the case of Poiseuille flow ($D = 1$) no symmetry-breaking bifurcation occurs, since the steady symmetric flow becomes unstable due to a Hopf bifurcation. For increasing expansion ratio Re_{c1} and Re_{c2} decrease. The calculations were done for expansion ratios up to $D = 1000$ and for this ratio the bifurcation points were found at $Re_{c1} = 8.5$ and $Re_{c2} = 11.2$. The results suggest that both $Re_{c1} \rightarrow 0$ and $(Re_{c2} - Re_{c1}) \rightarrow 0$ in the limit $D \rightarrow \infty$.

6.3. The limit case $D \rightarrow \infty$

For $D \gg 2$ the inlet height of the expansion can be considered small and the upper and lower walls of the outlet infinitely far remote; the inlet thus represents a line source discharging fluid into infinite semi-space. In this limit the flow can be treated by analytical means around the inlet source. There are two approaches available in the literature for dealing with this problem. The model given by Schlichting and Bickley (Schlichting 1968) makes use of the boundary layer equation and the assumption of a constant pressure imposed on the flow by the surrounding fluid. This assumption results in a constant momentum flux and an increasing mass flux in the x -direction. This model covers only the case of the flow in the half-space, the free jet. For the whole channel flow with a sudden enlargement, with constant mass flow resulting from a balance between outflow in the core and inflow in the recirculation periphery, this model is not suitable.

The other approach is based on the radial flow between two plane walls intersecting at an angle 2α , generated by a source or sink located on the line of intersection. Exact solutions of the Navier–Stokes equations, known as Jeffery–Hamel (JH) flows, are available for this problem (Schlichting 1968). Introducing plane polar coordinates (r, θ) and assuming radial flow

$$v_r(r, \theta) = \frac{1}{r} \frac{d\psi}{d\theta} \quad (6.1)$$

satisfying mass conservation with a streamfunction $\psi(\theta)$, the equations of motion

reduce to an ordinary differential equation in ψ :

$$\psi'''' + 4\psi'' + 2Re \psi' \psi'' = 0. \quad (6.2)$$

The boundary conditions

$$\psi(\pm\alpha) = \pm \frac{1}{3} \quad (6.3)$$

normalize the radial volume flux to $2/3$ between the walls, whereas

$$\left. \frac{d\psi}{d\theta} \right|_{\theta=\pm\alpha} = 0 \quad (6.4)$$

represents the no-slip condition for the velocity. Equation (6.2) can be solved analytically by Jacobian elliptic functions. Since the integration constants, which have to be determined from the boundary conditions, appear nonlinearly in the solution, it will be more convenient for our purpose to integrate equation (6.2) numerically.

For $\alpha = \pi/2$ the JH flow can be looked upon as a sudden expansion flow in the limits $d_2 \rightarrow \infty$ and $d_1 \rightarrow 0$, the flow pattern in the sudden expansion channel at $D \rightarrow \infty$ should look similar to the JH flow for

$$\frac{x^2 + y^2}{d_1^2} \gg 1. \quad (6.5)$$

The (normalized) net volume flux of the JH flow, defined by

$$Q_{JH} = \int_{-\pi/2}^{\pi/2} v_r(r, \vartheta) r d\vartheta = \frac{2}{3} \quad (6.6)$$

at $r = \text{const.}$, can also be obtained by integration of the horizontal velocity component

$$u_{JH} = v_r \cos \vartheta \quad (6.7)$$

along a vertical path, parallel to the wall situated at a distance x from it, as

$$Q_{JH} = \int_{-\infty}^{\infty} u_{JH} dy = \int_{-\pi/2}^{\pi/2} v_r(r, \vartheta) \cos \vartheta \frac{r(\vartheta)}{\cos \vartheta} d\vartheta, \quad (6.8)$$

with $r(\vartheta) = x/\cos \vartheta$. In figure 15 the comparison of the velocity profiles

$$u_{JH}(x, y) = v_r \left(\frac{x}{\cos \vartheta}, \vartheta \right) \cos \vartheta, \quad y = x \tan \vartheta \quad (6.9)$$

of the JH flow with those of the sudden expansion flow of $D = 1000$ is presented for various distances x , at a Reynolds number $Re = 1$.

When the JH velocity profile is compared with velocity profiles of sudden expansion flow calculated for finite values of d_1 and d_2 , good agreement can only be expected within a certain range of x . For $r = (x^2 + y^2)^{1/2} \rightarrow 0$ the velocity of the JH flow (equation (6.1)) becomes infinitely large. Therefore the JH flow overpredicts the velocity of the channel flow with a finite inlet height d_1 , when condition (6.5) is violated, i.e. close to the expansion. For $D = 1000$ and $Re = 1$ this is the case for $r < 5$ (see figure 15). With increasing distance x the no-slip condition for the velocity on the upper and lower channel walls increasingly influences the velocity profile, yielding to Poiseuille flow for $x \rightarrow \infty$, with its maximum velocity determined by the given, constant volume flux. Since the JH flow for $\alpha = \pi/2$ occupies the infinite semi-space, $u_{JH}(x, 0)$ decreases with increasing x , with $u_{JH}(x, 0) \rightarrow 0$ as $x \rightarrow \infty$, and the value for the maximum velocity of the JH flow eventually falls below that of

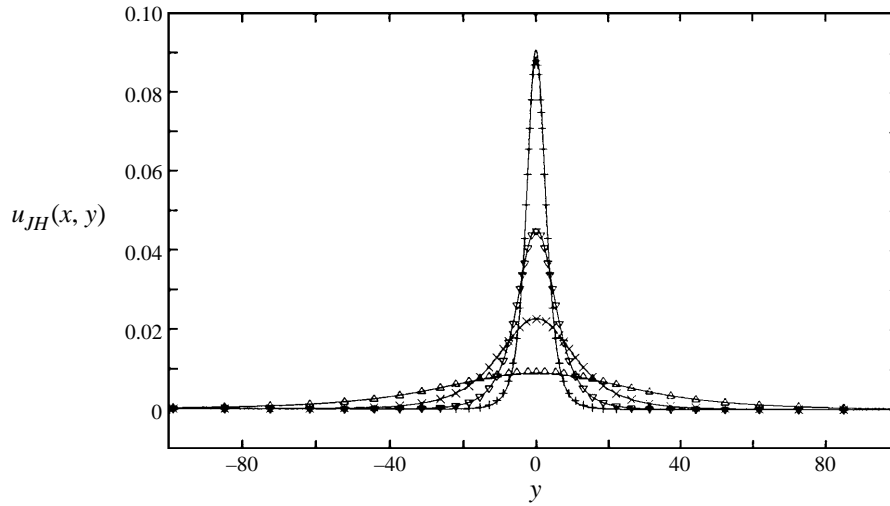


FIGURE 15. Comparison between the numerical results ($D = 1000$), and a Jeffery–Hamel flow (—) for $Re = 1$. +, $x = 5$; ∇ , $x = 10$; \times , $x = 20$; Δ , $x = 50$.

the channel flow beyond a certain distance x downstream of the expansion. For $D = 1000$ and $Re = 1$ the approximation of the channel flow by JH flow deteriorates significantly for $x \gg 50$ (see figure 15).

Sobey & Drazin (1986) found the stability limit for Jeffery–Hamel flows to be $Re_c = 0$ for $\alpha = \pi/2$. The Jeffery–Hamel flow at $Re = 1$ in figure 15 is therefore already unstable while the corresponding numerical results at $D = 1000$ are stable up to the critical point $Re_{c1} = 8.5$. According to the stability analysis of Sobey & Drazin (1986), the Jeffery–Hamel flow loses stability through a subcritical bifurcation while the symmetric sudden expansion shows a supercritical bifurcation. As pointed out in the previous paragraph, the two bifurcation points found for the sudden expansion flow move towards $Re = 0$ and their distance decreases as D is increased. A similar behaviour was found e.g. for Taylor–Couette flow (Pfister *et al.* 1987). There, the distance between two bifurcation points also decreases with increasing control parameter (aspect ratio for Taylor–Couette flow) and the first supercritical bifurcation point becomes subcritical at a certain value of the parameter and eventually merges with the second bifurcation point to form a higher-order singularity. Within the frame of the stability calculation of Sobey & Drazin (1986) and the numerical results of our work, such an effect, caused by the existence of the second bifurcation point, would possibly explain the subcritical bifurcation in the limiting case $D \rightarrow \infty$. Numerical evidence for this explanation, however, has not been found yet in the case of sudden expansion flow.

7. Conclusions

A systematic bifurcation analysis was carried out for flow in a channel with a sudden expansion. The numerical scheme applied confirmed the experimental and numerical results found by other researchers.

Weak viscous eddies, known as Moffatt eddies, were tracked in the corners of the expansion in the creeping flow limit, a fact neglected in previous studies. The numerically computed streamfunction was compared in the regions of the corner

vortices with an approximation formula derived by Moffatt (1964). The good agreement between both results served as an indicator for the accuracy of the numerical calculations.

Tracing the branch of unstable symmetric solutions beyond the first bifurcation point up to higher Reynolds numbers revealed a sequence of further bifurcation points. In order to answer the question of whether the flows emerging from the second (and higher) bifurcation points could be observed experimentally, their linear stability was investigated by a normal mode analysis. For the case of the second bifurcation point it could be shown that all solution branches intersecting at this point are unstable. The unstable symmetric branch, in particular, which has one unstable eigenmode for $Re < Re_{c2}$, remains unstable as the Reynolds number exceeds the critical value Re_{c2} and a second mode becomes unstable through a sign change of its growth rate at Re_{c2} . Therefore, an exchange of stability with an unstable branch becoming stable again at the second bifurcation point, as was observed e.g. in Pfister *et al.* (1987), does not occur for flows in a channel with a sudden expansion. Additional modes become unstable for the third and higher bifurcation points correspondingly.

Further bifurcation or limit points on the (stable) asymmetric branches arising from the first bifurcation point were not detected. This result is in accordance with all the publications which considered a sudden expansion with parabolic inflow and fully developed outflow boundary conditions. Contrasting with that, Sobey & Drazin (1986), who investigated a smooth expansion and contraction and periodic boundary conditions, found additional limit points on the non-symmetric solution branches. It is not clear if the differences are due to the *smooth* expansion/contraction or the *periodic* boundary conditions. For sufficiently long channels (i.e. long enough for the flow to reach a streamwise-invariant state within the expanded part of the channel before seeing the effect of contraction downstream), the effect of periodicity on the bifurcation structure should be minimal. Shapira *et al.* (1990) provide an estimate of the dimensionless development length downstream of an expansion as $L_e = 8 + 0.08Re$; for $Re = 100$ this yields a length of about 16 compared to a length of 80 used by Sobey & Drazin (1986). While the numerical results of Sobey & Drazin indicate that the estimate provided by Shapira *et al.* might be low, it is nevertheless clear that a length of 80 is sufficiently long for the flow to reach an invariant state (as seen in figure 4 of Sobey & Drazin). Calculations carried out by the authors for a channel with a distance of 80 between a sudden expansion and contraction, using fully developed inflow and outflow boundary conditions, yielded a bifurcation structure similar to those shown in figures 6, 12 and 13. The only other effect of periodicity is to provide a feedback to the inlet profile. This effect can be viewed as being equivalent to a non-periodic condition at the inlet, but with a different inlet condition than the parabolic profile that is normally used by all other researchers. Thus the differences in bifurcation structure (particularly the additional limit points observed on the non-symmetric branches and the evidence of two-dimensional time-periodic flows) can be attributed to either the *gradual* expansion or a *non-parabolic* inlet profile.

Shapira *et al.* (1990), however, considered a gradual slope with fully developed inflow and outflow boundary conditions and did not find such a complex bifurcation structure. This might suggest that the gradual expansion (a common feature in both Sobey and Drazin (1986) and Shapira *et al.* (1990)) is unlikely to be the cause of the complex bifurcation observed by Sobey & Drazin (1986), but periodicity (or non-parabolic inlet profile) is more likely to be the cause of multiplicity of stable,

non-symmetric solutions, as well as the time-periodic solutions at least over a narrow range of D .

The authors would like to thank Mr Richard Lehoucq for his valuable suggestions concerning the application of ARPACK. This work was supported in part by a scholarship of the Gottlieb Daimler- und Karl Benz-Stiftung the support is gratefully acknowledged.

REFERENCES

- ALLGOWER, E. L. & GEORG, K. 1990 *Numerical Continuation Methods — An Introduction*. Springer.
- CHERDRON, W., DURST, F. & WHITELAW, J. H. 1978 Asymmetric flows and instabilities in symmetric ducts with sudden expansions. *J. Fluid Mech.* **84**, 13–31.
- CHU, E., GEORGE, A., LIU, J. & NG, E. 1984 SPARSPAK. *Research Rep.* CS-84-36, University of Waterloo.
- COLLINS, W. M. & DENNIS, S. C. R. 1976 Viscous eddies near a 90° and a 45° corner in flow through a curved tube of triangular cross-section. *J. Fluid Mech.* **76**, 417–432.
- DURST, F., PEREIRA, J. C. F. & TROPEA, C. 1993 The plane symmetric sudden-expansion flow at low Reynolds numbers. *J. Fluid Mech.* **248**, 567–581.
- FEARN, R. M., MULLIN, T. & CLIFFE, K. A. 1990 Nonlinear flow phenomena in a symmetric sudden expansion. *J. Fluid Mech.* **211**, 595–608.
- KELLER, H. B. 1987 *Numerical Methods in Bifurcation Problems*. Springer.
- LEHOUCQ, R. B., SORENSEN, D. C. & VU, P. ARPACK: An implementation of the Implicitly Restarted Arnoldi Iteration that computes some of the eigenvalues and eigenvectors of a large sparse matrix. Available from netlib@ornl.gov under the directory scalapack.
- MOFFATT, H. K. 1964 Viscous and resistive eddies near a sharp corner. *J. Fluid Mech.* **18**, 1–18.
- NATARAJAN, R. & ACRIVOS, A. 1993 The instability of the steady flow past spheres and disks. *J. Fluid Mech.*, **254**, 323–344.
- PFISTER, G., SCHMIDT, H., CLIFFE, K. A. & MULLIN, T. 1987 *Bifurcation Phenomena in Taylor–Couette Flow in a very Short Annulus*. TP.1209, Theoretical Physics Division, Harwell Laboratory.
- ROACHE, P. J. 1972 *Computational Fluid Dynamics*. Hermosa.
- SAAD, Y. 1992 *Numerical Methods for Large Eigenvalue Problems*. Halsted.
- SCHLICHTING, H. 1968 *Boundary Layer Theory*, 6th edn. McGraw Hill.
- SHAPIRA, M., DEGANI, D. & WEIHS, D. 1990 Stability and existence of multiple solutions for viscous flow in suddenly enlarged channels. *Computers & Fluids* **18**, 239–258.
- SOBEY, I. J. & DRAZIN, P. G. 1986 Bifurcations of two-dimensional channel flows. *J. Fluid Mech.* **171**, 263–287.
- TESCHAUER, I. 1994 Numerische Untersuchungen der symmetriebrechenden Bifurkation bei Strömungen durch plötzliche Kanalerweiterungen. Studienarbeit, Lehrstuhl für Strömungsmechanik, Universität Erlangen–Nürnberg.